CHAPTER TEN

Primary Structures of Iron Meteorites

The Widmanstätten Structure

The Widmanstätten structure has puzzled geologists and metallurgists ever since it was revealed by Alois von Widmanstätten and G. Thompson independently in 1808. Some historical aspects have been touched upon in this work when describing Elbogen, Lenarto, and Hraschina. Other aspects were discussed by Paneth (1960), C.S. Smith (1960; 1962) and Mehl (1965). The Widmanstätten structure is characteristic for a major group of iron meteorites, the octahedrites; and it also occurs in many anomalous irons, e.g., Netschaevo, and in mesosiderites, e.g., Mount Padbury. It is present on a microscopic scale in very many meteorites and in technological alloys, e.g., cast α - β brasses, welded joints in steels and tempered Al-Ag alloys.

There was a time when it was believed that the Widmanstätten structure of iron meteorites had formed directly by crystallization from a very slowly cooling melt. Smith (1855), Tschermak (1875), Sorby (1877), Cohen (1894: 83), and Vogel (1927; 1932) were the foremost supporters of this theory. As they saw it, the structure was in accordance with observations of crystallizing ice and even with the ternary Fe-Ni-P diagram as developed by Vogel & Baur (1931).

Osmond & Cartaud (1904) were the first to show that the Widmanstätten structure must have formed at temperatures that were at least 700° C lower than the melting temperatures and that the process was one of solid state diffusion. For many years it appeared, however, that metallurgists did not clearly recognize the differences between the meteoritic Widmanstätten structure, due to extremely slow cooling, and the so-called Widmanstätten structure claimed to have been produced artificially in nickel-iron. The reports by Belaiew (1910), Benedicks (1910), Mehl & Derge (1937), Buddhue (1948) and many others, thus, do not concern true Widmanstätten structures, but α_2 and martensitic structures obtained in the laboratory by furnace cooling or quenching of austenitic nickel-iron. The true Widmanstätten structure forms by a diffusion-controlled nucleation and growth process that is slow even on a geological time scale. The kamacite (ferrite) preferentially nucleates along the octahedral planes of the parent taenite (austenite) phase. The Widmanstätten pattern is developed when the individual plates or bands of kamacite thicken by solid state diffusion and eventually touch one another. In octahedrites at least some traces of the high-nickel taenite precursor phase will almost always remain, usually as discrete blebs, wedges or platelets. In addition, the microscopic mixture of α and γ, plessite is usually present as a hallmark of meteorites with between six and 20% Ni.

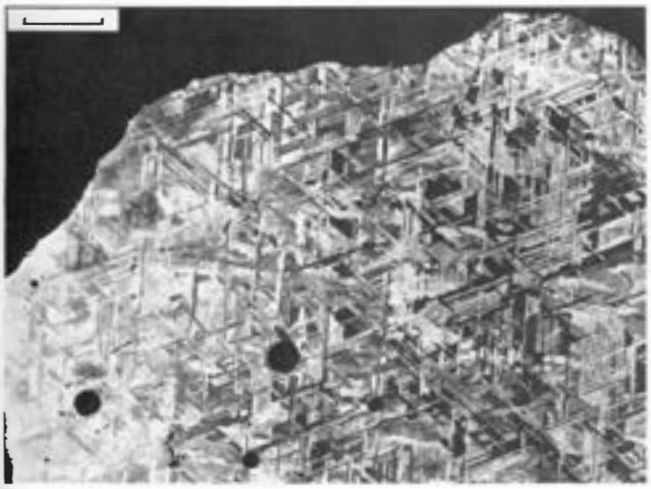

Figure 179. Casas Grandes (U.S.N.M. no. 369). Typical Widmanstätten structure of a medium octahedrite. The oriented sheen is mainly due to the different crystallographic orientations of the individual kamacite lamellae. Two large and several smaller troilite inclusions. Deep-etched. Scale bar 50 mm. (From Merrill 1916a: plate 16.)

The early attempts to interpret the Widmanstätten structure were restrained by the imperfectly known binary Fe-Ni diagram which was usually thought to contain a eutectoid at 17-30% Ni and 350° C. See, e.g., Osmond & Cartaud 1906; Pfann 1918; Perry 1944: 38. Also, in meteorites, the abundant occurrence of schreibersite caused Vogel (1952) to maintain that the majority of the phosphides had been formed from a liquid phase which persisted down to temperatures of about 970° C. Various distorted Fe-Ni-P diagrams have thus been in current use until the mid-1960s (e.g., Goldstein & Ogilvie 1963; Reed 1965a; Axon 1968a).

However, with the presentation of the binary Fe-Ni diagrams of Owen & Sully (1939) and Owen & Burns (1939), the stage was set for a more thorough understanding so that Perry (1944: 43, etc.) could present a qualitatively correct picture. Improved binary diagrams (Owen & Liu 1949; Goldstein & Ogilvie 1965a) and ternary diagrams (Buchwald 1966; Doan & Goldstein 1970) are now available and necessary in order to comprehend fully the various aspects of the Widmanstätten structure. For data see Table 33 and Figures 181-184.

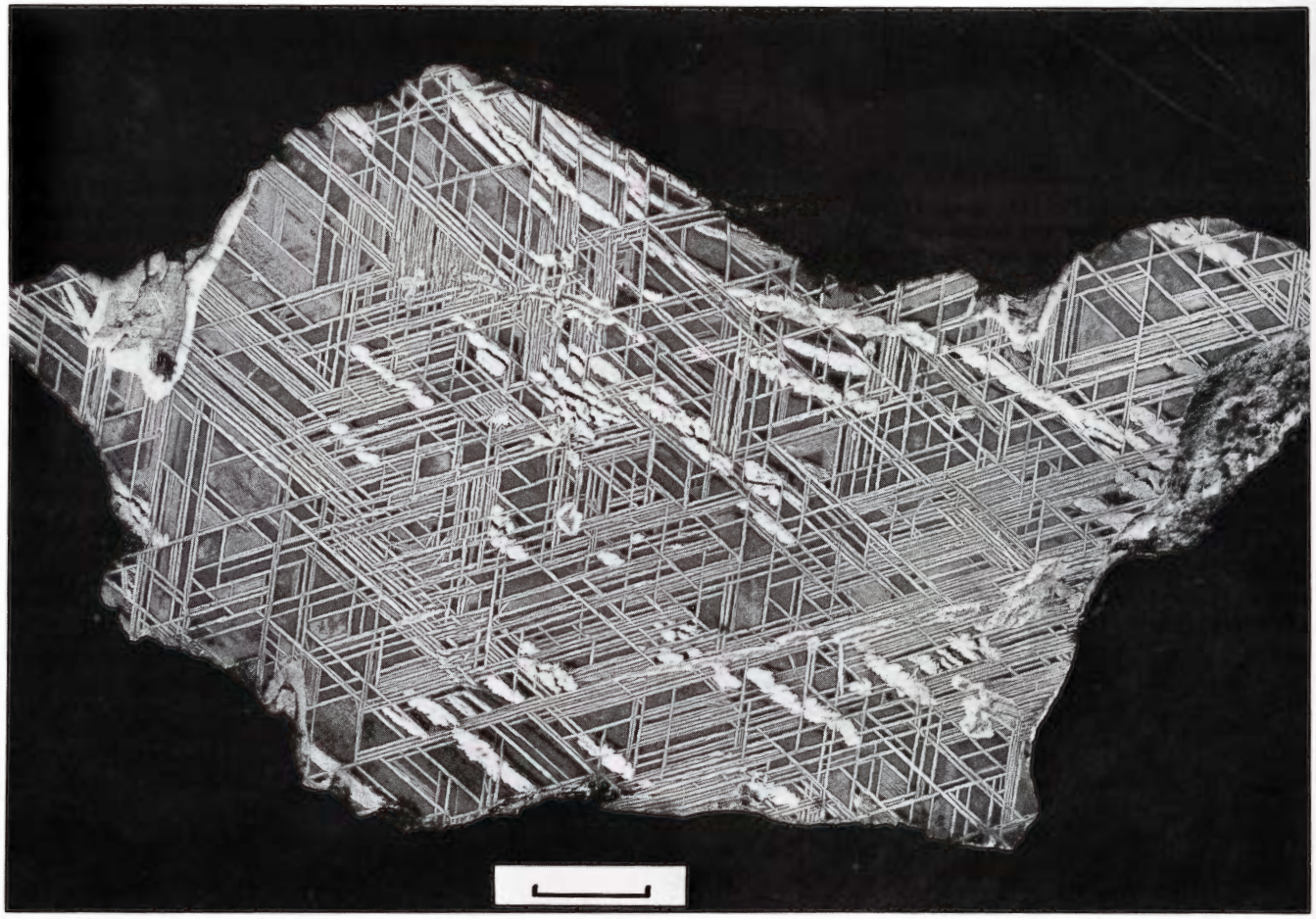

Figure 180. Edmonton (Kentucky) (U.S.N.M. no. 1413). Typical Widmanstätten structure of a fine octahedrite. Three $\{111\}$ directions form angles of 60°, while the fourth set of kamacite lamellae are almost parallel to the plane of section and appear as irregular white plumes. Large schreibersite crystal with swathing kamacite to the left. Deep-etched. Scale bar 20 mm. S.I. neg. M-375.

It has even been possible, experimentally, to nucleate Widmanstätten kamacite in synthetic Fe-Ni-P alloys with 0.1-0.4% P (Buchwald, unpublished research; Goldstein & Doan 1972). Kamacite will first form as discrete blebs on grain boundaries then, at about 50° lower, as a Widmanstätten grid in the homogeneous grain interior. The individual kamacite laths are narrow, about 1-10 μ; although phase separation on a scale as large as that found in meteorites cannot be produced in the laboratory, the trend seems to be clear.

The observation made by Osmond & Cartaud (1904; 1906) about solid state decomposition is generally applicable to cooling metallic systems. When a solid solution, stable at high temperatures, precipitates a new phase upon cooling, this new phase appears in a particular manner. It deposits in such a way that its lattice bears a definite crystallographic relation to the lattice of the parent solid solution. Young (1926) showed that the crystallographic relationship in question was

$$\{111\}_\gamma \parallel \{110\}_\alpha$$
$$[110]_\gamma \parallel [111]_\alpha$$

This was further supported by studies of Böggild (1927), Mehl & Barrett (1931) and Mehl & Derge (1937). The α-lamellae run parallel to the four planes defined by the faces of an imaginary octahedron, and for this reason iron meteorites displaying the Widmanstätten pattern are called octahedrites. The problem of predicting the angles of the Widmanstätten pattern on a section through the meteorite has been analyzed by various authors, e.g., Tschermak

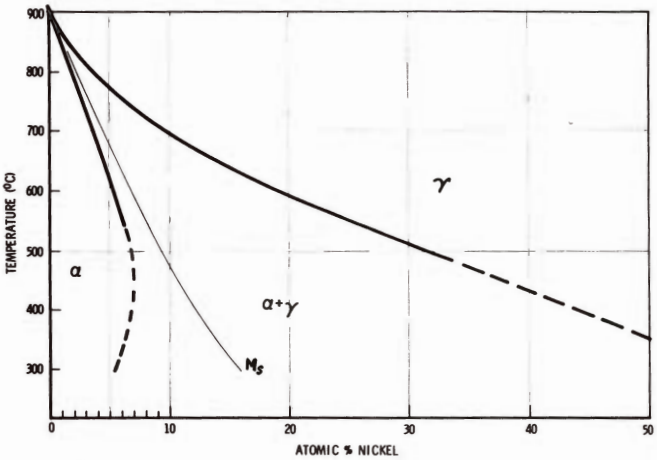

Figure 181. The Fe-Ni phase diagram. Broken lines indicate extrapolations to temperatures where experimental equilibrium was not obtained. The thin line, M_S, indicates the start of martensitic transformation to α_2 under non-equilibrium conditions. (From Kaufman & Cohen 1956; Goldstein & Ogilvie 1965a.)

(1871b), Brezina (1882), Leonhardt (1928) and Hey (1942). A set of tables was recently prepared by Buchwald (1968b).

Cooling Rates

With the advent of the electron microprobe it finally became possible to analyze the detailed composition of kamacite and taenite and, from experimentally determined diffusion coefficients for the Fe-Ni system, to estimate the cooling rates of meteorites. Qualitative predictions had been presented by Uhlig (1954) and Urey (1956). Then quantitative data and interpretations were accumulated in works by Maringer et al. (1959), Massalski & Park (1962), Wood (1964), Short & Andersen (1965), Goldstein & Short (1967), Fricker et al. (1970) and Goldstein & Doan (1972). For the determination of cooling rates, the measured Ni concentration gradients in the taenite that result from the growth of the Widmanstätten pattern are compared with the calculated nickel gradients obtained from a computer simulation of the growth process. The absolute values of the cooling rates range from 0.4° C to 500° C per million years. The cooling rates are only valid for the region in which the Widmanstätten pattern forms – i.e., 700-450° C. Typical estimates are given in Table 34.

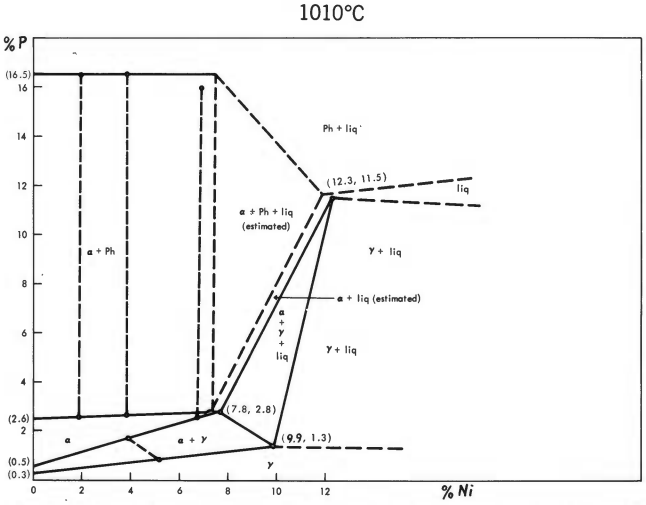

Figure 182. Isotherm section through the ternary Fe-Ni-P phase diagram 10° above the ternary reaction plane. (From Doan & Goldstein 1970.)

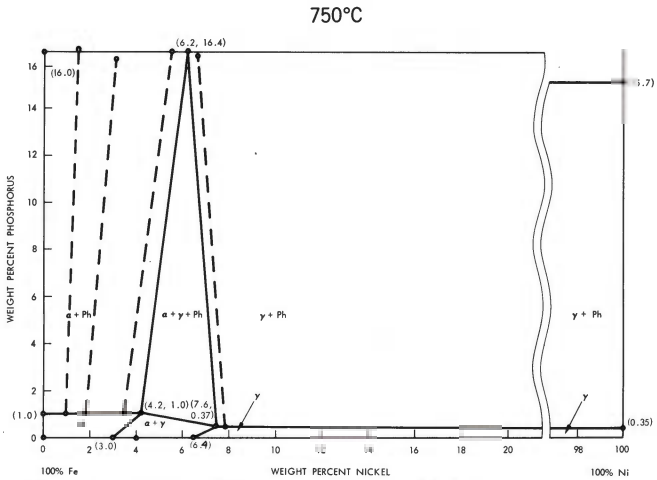

Figure 183. Isotherm section through the Fe-Ni-P diagram at 750° C. (From Doan & Goldstein 1970.)

Table 33. Equilibrium Phase Data for the Ternary Fe-Ni-P System

	α		γ		Ph		Liquid	
Temperature, °C	Weight % Ni	Weight % P	Weight % Ni	Weight % P	Weight % Ni	Weight % P	Weight % Ni	Weight % P
1100	6.25±0.2	2.5±0.1	7.6±0.2	1.15±0.1			9.9±0.3	12.8±0.5
(1100)	(4.5)	(2.0)	(7.7)	(1.25)			(10)	(9)
1080	6.65±0.2	2.6±0.2	8.7±0.15	1.2±0.1			8.4±1.8	12.0±1.0
1070	7.2±0.2	2.55±0.1	9.1±0.1	1.2±0.1			10.7±2.0	12.5±0.8
1060	6.9±0.3	2.50±0.1	8.9±0.3	1.2±0.1			11.3±1.0	13.5±0.8
1040	7.4±0.2	2.7±0.1	9.4±0.2	1.3±0.1			10.7±1.0	11.7±1.0
1025	7.3±0.3	2.7±0.1	9.3±0.1	1.3±0.1			11.4±1.0	11.5±1.0
1010	7.8±0.1	2.8±0.1	9.9±0.1	1.3±0.1			12.3±1.0	11.5±1.0
1000	7.5±0.1	2.7±0.1	9.8±0.1	1.4±0.1	8.0±0.1	16.5±0.5	11.5±1.0	12.5±1.0
Four-phase reaction plane								
(970)	(4.5)	(2.0)	(9.0)	(1.2)	(4.5)	(15.5)	(12)	(10)
Four-phase reaction plane								
975	6.6±0.1	2.3±0.1	8.8±0.1	1.1±0.05	7.0±0.15	16.2±0.5		
(950)	(4.5)	(2.0)	(8.5)	(1.1)	(6.0)	(15.5)		
925	5.6±0.1	2.05±0.1	7.7±0.1	0.9±0.05	6.2±0.15	16.3±0.5		
875	4.3±0.1	1.7±0.15	6.7±0.2	0.75±0.1	5.2±0.4	16.1±0.5		
(875)	(4.5)	(2.0)	(7.0)	(0.8)	(10.0)	(15.5)		
850	4.2±0.1	1.55±0.05	6.50±0.1	0.65±0.03	5.25±0.1	16.1±0.3		
750	4.2±0.2	1.03±0.03	7.6±0.5	0.37±0.02	6.2±0.2	16.4±0.5		
(750)	(4.0)	(1.3)	(7.0)	(0.65)	(8.0)	(15.5)		
700	4.7±0.2	0.65±0.1	9.5±0.5	0.27±0.03	8.4±0.5	15.5±0.5		
650	5.3±0.3	0.5±0.05	11.0±0.5	0.15±0.04	10.5±0.5	15.5±0.5		
(650)	(3.8)	(0.6)	(14)	(0.3)	(16)	(15.5)		
600	5.5±0.5	0.32±0.04	15±2.0	0.12±0.02	15±2.5	15.5±1.0		
550	7.4±0.4	0.26±0.02	19±3.0	0.08±0.02	~19±3	>13.3		
(550)	(5.5)	(0.4)	(24)	(0.1)	(24)	(15.5)		

Data in parenthesis from Buchwald (1966), the remainder from Doan & Goldstein (1970).

Figure 188 summarizes the development of the Widmanstättten structure from an initially homogeneous high-temperature γ-phase with e.g., 10% Ni. The homogeneous taenite phase may have been produced by melting and solidification, but may as well have been produced by sintering and annealing inside the taenite field of the equilibrium diagram. Probably both cases occur within the field of meteorites. Some group I irons and some anomalous irons (e.g., Barranca Blanca) do not ever seem to have been melted, while on the other hand, group IIIA-IIIB, e.g., Cape York, and group IVA, e.g., Gibeon, almost certainly have passed through a completely molten stage.

In the development of the theory of cooling rates various assumptions are made. First, it is assumed that new kamacite does not precipitate immediately when the

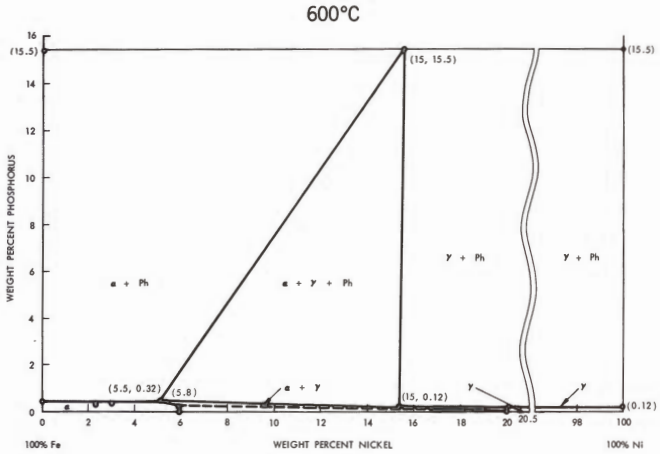

Figure 184. Isotherm section through the Fe-Ni-P diagram at 600° C. (From Doan & Goldstein 1970.)

Table 34. Estimated Cooling-rates (Goldstein 1969)

Group	Cooling rate range °C per 10^6 years
I	1 - 3
IIC	65 - 250
IIIA	1.5 - 10
IIIB	1 - 2
IVA	7 - 80
IVB	2 - 20

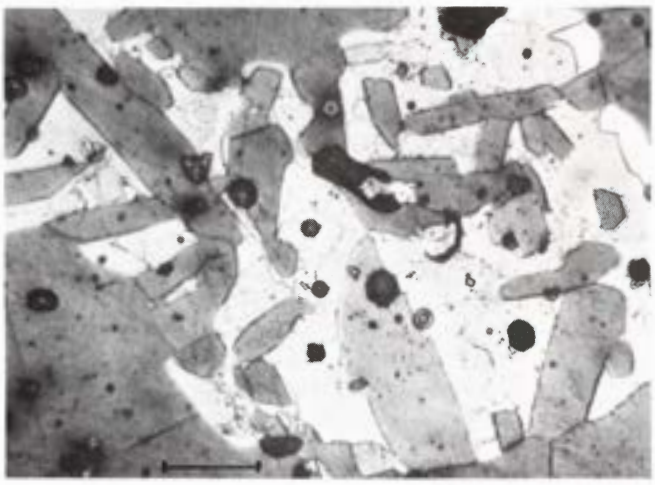

Figure 185A. Widmanstätten structure in a synthetic alloy with 3% Ni and 0.9% P. Upon cooling from homogenization at 1100° C (70 hours), the austenite started decomposition to ferrite lamellae (dark) and retained austenite (light) when kept for 71 hours at 760° C. Etched. Scale bar 30 μ.

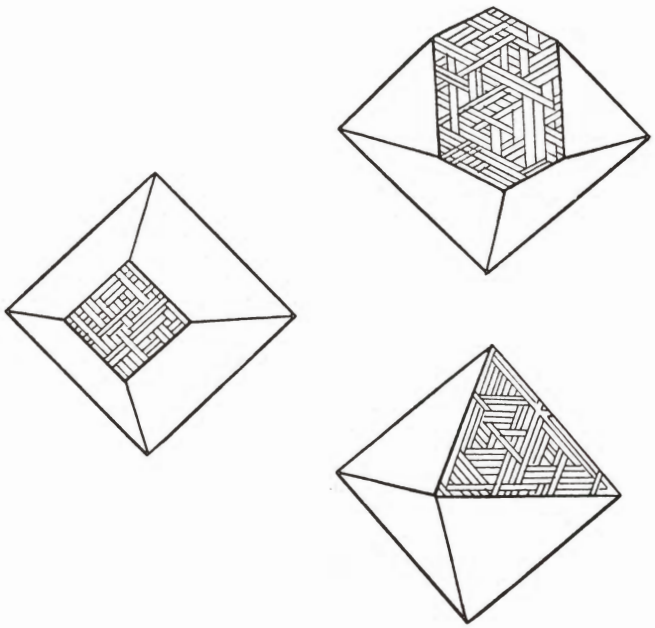

Figure 185B. Sketches by Tschermak (1894) of the Widmanstätten structure as it would appear on sections parallel to $(100)_\gamma$, $(110)_\gamma$ and $(111)_\gamma$ of the parent taenite crystal.

Figure 186. Cape York (Agpalilik) (Copenhagen no. 1967, 410). A cube has been accurately cut, so that all faces are parallel to (100) of the parent taenite crystal. On all faces the kamacite lamellae run in only two directions, as diagonals. A troilite inclusion, elongated after $[100]_\gamma$, is also seen. Length of edge 68 mm; weight 2,418 g. The specific gravity, 7.69 g/cm^3, is low as the result of about 7 volume % troilite inclusions.

$\gamma/\gamma + \alpha$ boundary is crossed during cooling. Thus, on the one hand, it is maintained that the cooling rates are extremely low; therefore, one would expect equilibrium conditions to prevail at 700° C. On the other hand, it is argued that the nucleation process is so difficult that significant undercooling is required. Therefore, 50°-100° C undercooling – i.e., a lapse of several million years – is assumed on the grounds that this gives the best agreement between computed and experimental M-profiles. If the system was at complete undisturbed isolation one might perhaps accept an appreciable undercooling. On a celestial body of some size it appears, however, that relative displacements could have occurred, thereby introducing distorted regions which could serve as nucleating sites. Movement of the overburden could have occurred both as the result of collapse of cavities caused by melting and shrinkage, and as the result of shock events on the surface.

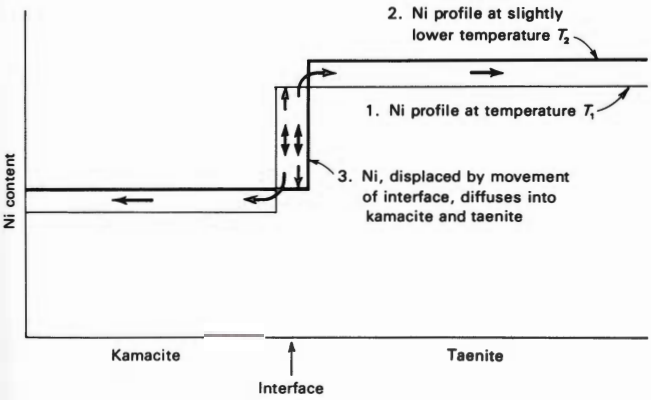

Figure 187. Diagram showing diffusion of nickel from interface regions to interiors of crystals in cooling octahedrites. (From Wood 1968.)

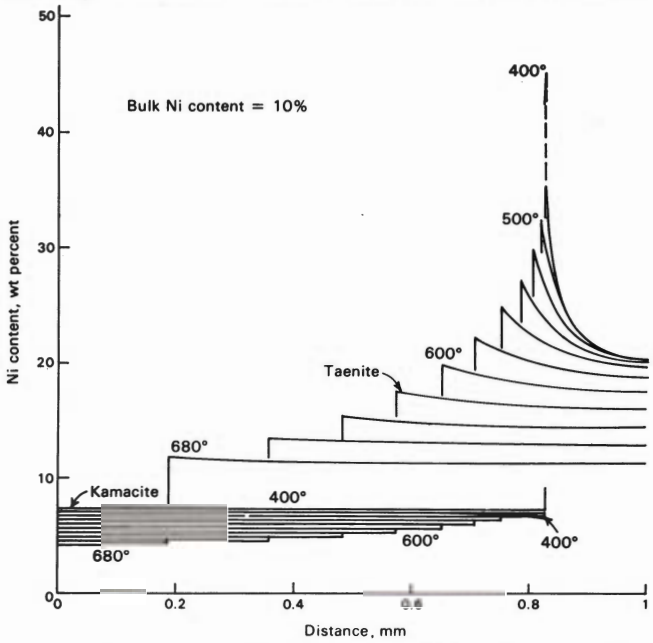

Figure 188. The computed development of Ni profiles in a cooling octahedrite. Left edge of figure represents midpoint of a kamacite lamella; kamacite expands and increases in Ni content as temperature falls. Right edge of figure is center of a residual taenite area. Here, the Ni content also increases, at first throughout the taenite, later along edges only. Final result is an M-shaped profile, like those shown in Figure 107. (From Wood 1968.)

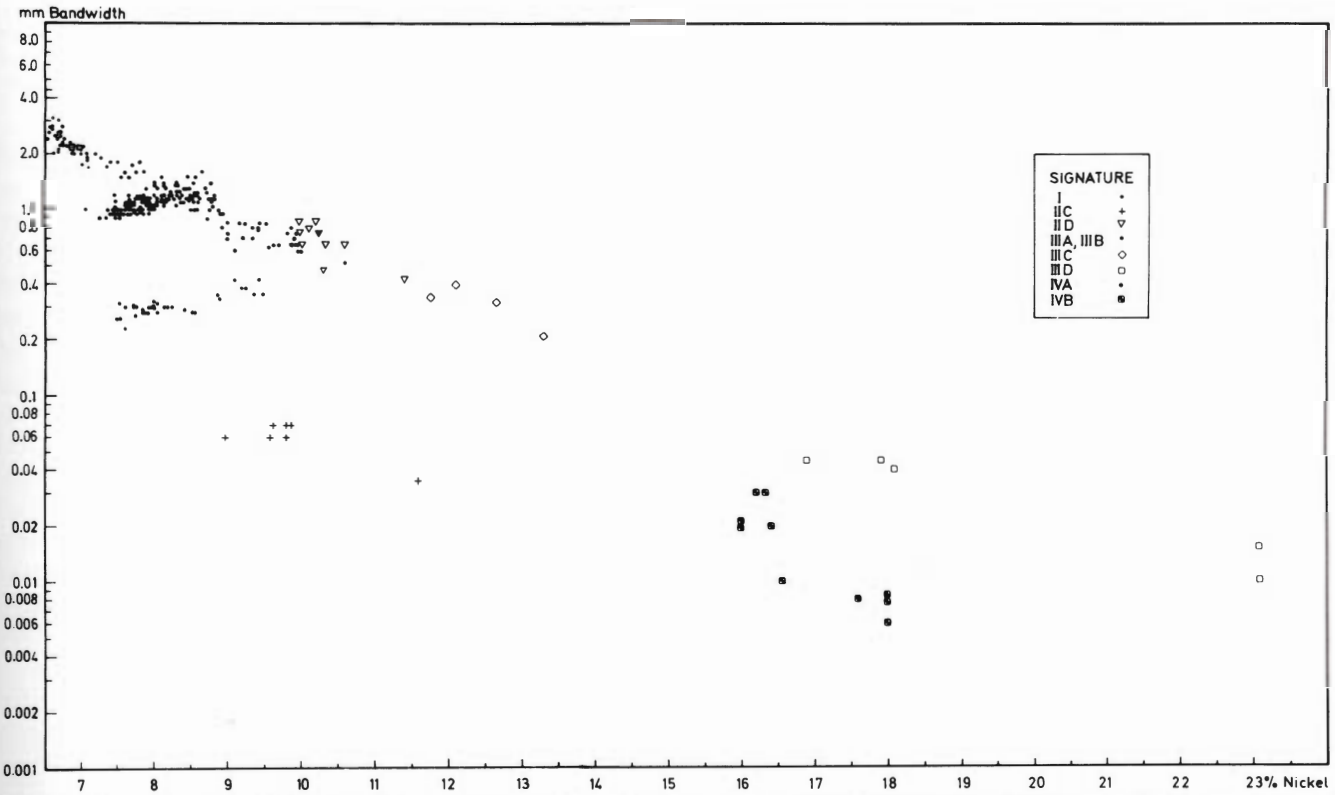

Figure 189A. Kamacite bandwidth versus nickel percentage in iron meteorites. Each point represents one meteorite, and the chemical group is given. Also included are data from some ataxites (IVB) with narrow α-spindles. Data have been taken from the descriptive part.

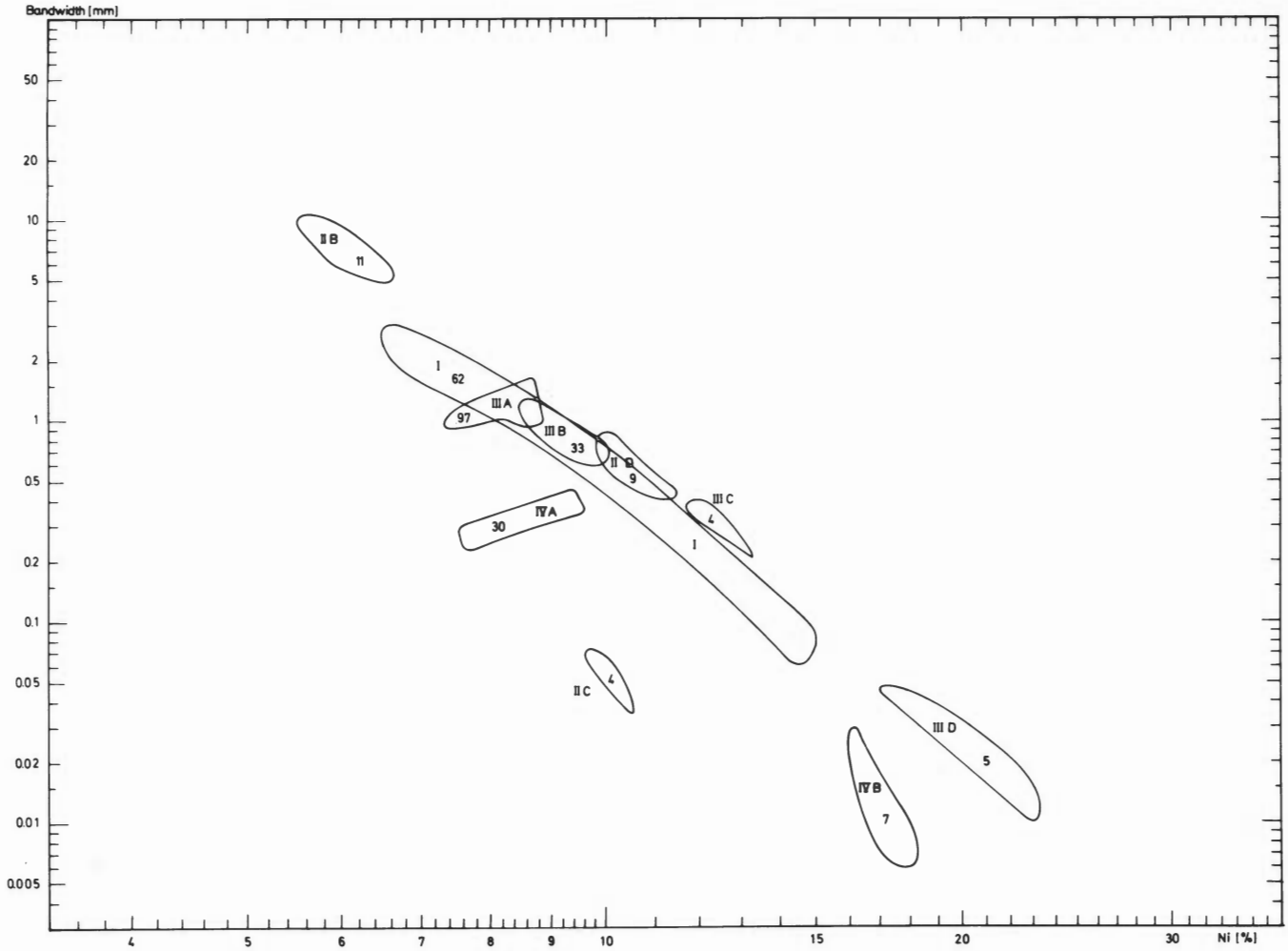

Figure 189B. Log-log plot of kamacite bandwidth versus nickel percentage. Within the groups the bandwidths are inversely proportional to the nickel percentage. Group IIIA and IVA apparently are exceptions. Compare the distinct clustering here with that obtained when using Ni-Ga or Ni-Ge plots (Figures 79 and 80) as a classification basis. For up-to-date numbers within each group, please see Table 27.

There are other assumptions which perhaps are less questionable, e.g., the exact boundaries of the Fe-Ni phase diagram, the change of these boundaries with slightly elevated pressures and alloying elements the activation energies and the extrapolation of diffusion coefficients to low temperatures. The superposition of secondary structures caused by cosmic (or artificial) reheating can also pose many problems not usually taken into account. The influences of P, Co and C on the diffusion processes are difficult to explain quantitatively. Meteorites with less than 7% Ni cannot be considered in cooling rate calculations because taenite and plessite occur in too small amounts or not at all.

Nevertheless, the cooling rates are apparently semi-quantitatively correct, and the observation of differences of cooling rate between different resolved chemical groups is certainly valid. In the future, independent lines of evidence should be looked for in order to support the cooling rate data.

It has been estimated that the cooling rates of the observed sizes would be characteristic of asteroidal-sized bodies, 10-800 km in diameter. Wood (1964) estimated that a planetary body greater than about 850 km would thus not cool to below 500° C at the center within the age of the solar system. Therefore, any proposed parent body seems to be restricted to dimensions comparable with asteroids (Table 2) rather than the Moon or Earth (Table 1). This conclusion is supported by the evidence against pressures of greater than a few k bars in the parent body. The arguments put forward by Uhlig (1954), Urey (1956), Ringwood (1960) and Carter & Kennedy (1964) in favor of high hydrostatic pressures (30-50 k bar or higher) have all been discredited in a number of papers by Nininger (1956), Lipschutz & Anders (1961; 1964), Anders (1964) and Brett & Higgins (1967), to name a few. Even it it is difficult to set a precise upper limit for the pressures in the primordial bodies, it is now generally agreed that pressures above 10 k bar are highly unlikely.

A Typical Example From Group III

From the solidification ages, page 138, it would seem that many iron meteorites went through a liquid state about 4.5×10^9 years ago. From the cosmic ray exposure ages, it would appear that the solidified and cool bodies

Figure 189C. Cape York (Agpalilik) (Copenhagen no. 1967, 410). A slice measuring 180 x 125 x 5 cm has been polished on one side and slightly etched in one half of the picture. The oriented troilite inclusions are obvious. A comparison with Figure 158, which shows a parallel surface 55 mm distant, reveals that no inclusions are common to both slices. Other sections, perpendicular to those shown, and X-ray photographs, corroborate the conclusion that the troilite crystals are sausage-shaped with maximum thicknesses of about 5 cm. The ruler measures 100 cm.

fragmented about 0.5×10^9 years ago. Thus a time interval of about 4×10^9 was available for the irons to solidify and cool to below 400° C when almost all diffusion processes in the Fe-Ni-P system – with the minor additional elements C, S, Si, Cr, etc. – ceased to be operative.

Let us examine the primary structure of a typical iron meteorite of group IIIA-IIIB, with information derived from Rowton, Cape York, Juncal, Kouga Mountains and Chupaderos.

I. These iron meteorites are nearer in character to directionally solidified single crystals than to ordinary castings. Cape York, e.g., was, about 700° C, a single austenite crystal more than 200 cm in diameter. The presence of large, parallel troilite inclusions, corresponding to a bulk S-content of 1.3%, indicates that the mass solidified slowly in one direction. Moreover, the troilite pockets are all parallel to $[100]_\gamma$, a known growth direction of austenite. While the metallic solidification front advanced, the sulfides were trapped in elongated interstices in the metal. Many chromite and phosphate crystals were washed out of the original heterogeneous material and are now to be found enclosed in the large troilite nodules. Whether a major portion of these oxygen-containing minerals was formed at the time of melting, thus capturing the oxygen from the metal – or whether they were just mechanically removed from the metal at this time – is not clear yet.

The trapped minerals are usually concentrated at one and the same end of the troilite, suggesting the presence of an active gravity field during solidification or at least supporting the other evidence for a large scale directional solidification. It is possible that only a minor portion of the entire primordial material was heated above 1500° C and melted at any one time. The process may perhaps have been comparable to zone melting, a possibility which has been examined by Fricker et al. (1970).

II. Upon cooling from about 1400° C the material became thoroughly homogenized with respect to Fe, Ni, Co, C, P, etc. The taenite slowly became supersaturated with respect to chromium that precipitated as chromite lamellae parallel to $100\}_\gamma$. Any sulfur in solid solution also precipitated, either as minute angular troilite particles or as shapeless troilite sheets nucleated by the chromite-taenite interfaces.

III. In the range of 900°-700° C a major part of the phosphorus, previously in solid solution in the taenite, precipitated as schreibersite. Favorable nucleation sites were (i) original taenite grain boundaries and the incoherent parts of the twin boundaries, and (ii) inclusions such as troilite, chromite, phosphates and – in group III only rarely – silicates. Nevertheless, homogeneous nucleation (iii) may also have occurred but perhaps only as an exception to the rule.

Although theoretically well founded, case (i) is mainly speculation. Most iron meteorites of group IIIA-B are composed of huge parent austenite crystals in which grain

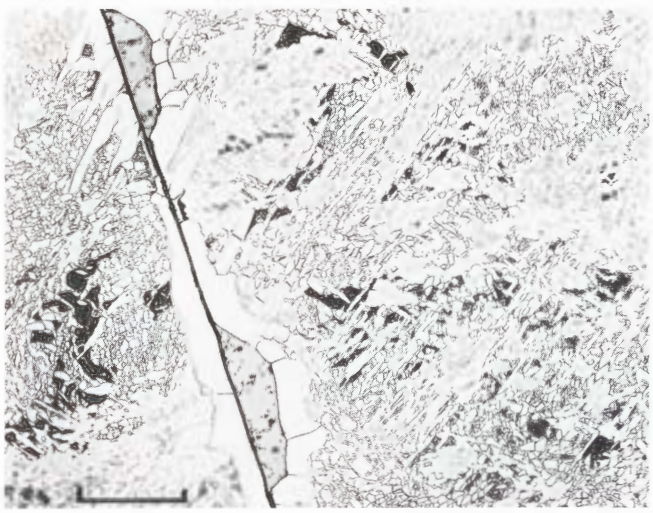

Figure 190. Monahans (Copenhagen 1966, 141). A thin straight chromite lamella has served as a substrate for two troilite blebs (gray). Upon further cooling, kamacite nucleated here and formed a swathing rim. Some Widmanstätten growth of the ferrite was apparently rapidly stopped. Etched. Scale bar 200 μ.

and twin boundaries only rarely are revealed by cutting. One good exception is Savannah, page 1088. Outside group III, Santa Rosa, page 1075, and Toluca, page 1209, may be cited. Case (ii), however, is very commonly observed. The large troilite inclusions nucleated copious schreibersite rims that grew to thicknesses of 0.1-1.5 mm, the final thickness reflecting the bulk phosphorus content of the meteorite. Also, the small troilite, chromite and phosphate crystals became enveloped by schreibersite – often to such an extent that the original nuclei became entirely swamped. (iii) Some schreibersite precipitated in the taenite grain interiors as Brezina lamellae oriented parallel to $\{110\}_\gamma$. In very many cases it appears that the nucleation was not truly homogeneous but was aided by minute troilite, chromite and phosphate particles.

IV. Swathing kamacite started to form around many heterogeneous nuclei, when – depending on nickel content – the cooling parent body finally moved into the two-phase $\alpha + \gamma$ region of the equilibrium diagram. Or, with more phosphorus, it moved into the three-phase ($\alpha + \gamma$ + phosphide) region. The swathing kamacite grew to 0.5-2 mm widths around troilite, chromite and schreibersite. It also precipitated along primary taenite grain boundaries. The swathing kamacite is often composed of several kamacite grains, each developed from a different nucleus. Its formation may have been aided by Ni and P depletion around the primary schreibersite crystals, but this depletion was not necessary since swathing kamacite also formed around troilite, chromite and – in pallasites, etc. – around silicates.

V. With the important solid-state reactions, that took place between about 725° C and 500° C, the meteorite finally acquired its characteristic macro- and microstructure.

a. The swathing kamacite of IV had grown appreciably, when – upon further cooling for 50° C or 100° C – the Widmanstätten structure started to appear. Depending on the actual nickel and phosphorus content it nucleated at about 725° C to 700° C. It evidently nucleated homogeneously in the grain interiors, simultaneously in many places. As the oriented kamacite lamellae grew, the nickel surplus was pushed into the residual taenite which also accommodated a major part of any carbon in solid solution. The Widmanstätten pattern was probably fully developed at around 450° C after which no further bulk diffusion could occur. Simultaneously with its formation, phosphorus – previously in solid solution – precipitated along the α - α and α - γ interfaces as irregular schreibersite particles and, in the kamacite lamellae, as prismatic rhabdites. In general, the smaller particles were precipitated at lower temperatures and became richer in nickel, in accordance with the experimentally determined Fe-Ni-P diagram. Imperfect regulation of the nickel content of the primary schreibersite bodies towards higher nickel content also occurred.

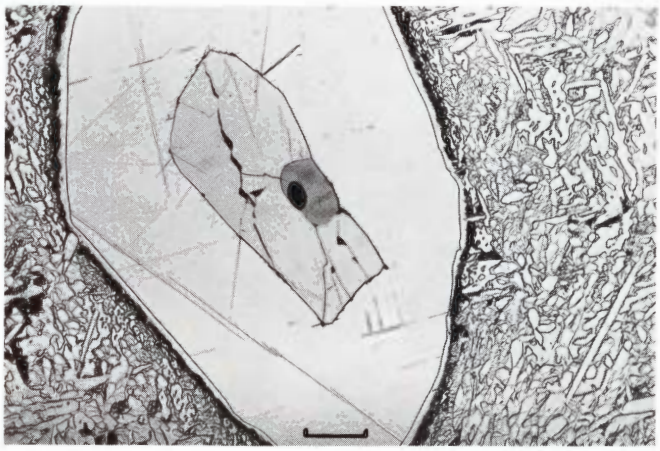

Figure 192. Wiley (Tempe no. 380.1x). Nucleation problems play a major role within meteoritic transformation processes, but this is usually overlooked. The sequence of precipitation here was: phosphate (black), troilite (dark gray), schreibersite (gray) and kamacite (white). Each phase nucleated the following. Etched. Scale bar 50 μ.

Figure 191. Chupaderos (the Cuernavaca sample in Chicago no. 1025). Brezina lamellae of schreibersite. Rough grinding and polishing has caused them to stand in low relief. Note the well-preserved fusion crust and a hole left by troilite which ablated. Deep-etched. Scale bar 20 mm.

Figure 193. Cape York (Agpalilik) (Copenhagen no. 1967, 410). Etched portion of Figure 189, turned 90°. The Widmanstätten structure is well developed, and since the slice is parallel to $(100)_\gamma$ only two diagonal kamacite directions are seen. Troilite appears black. Scale bar 40 mm.

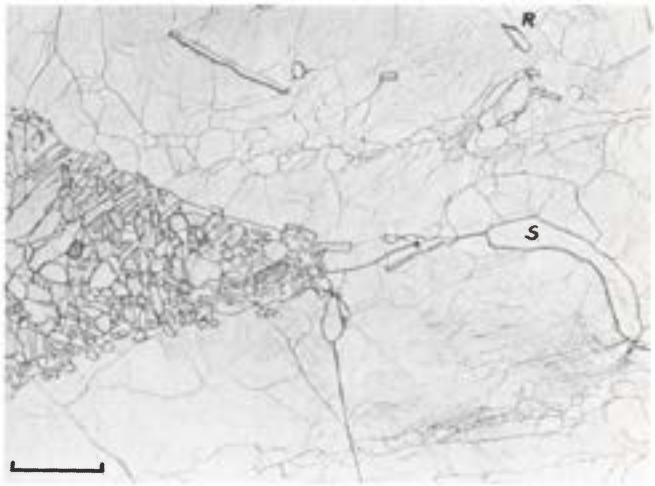

Figure 194. Providence (U.S.N.M. no. 1340). Subboundaries occur in the kamacite of all iron meteorites. In this particular one the array is confusing and extraordinary. Schreibersite (S), rhabdite (R) and a plessite field to the left. Etched. Scale bar 200 μ.

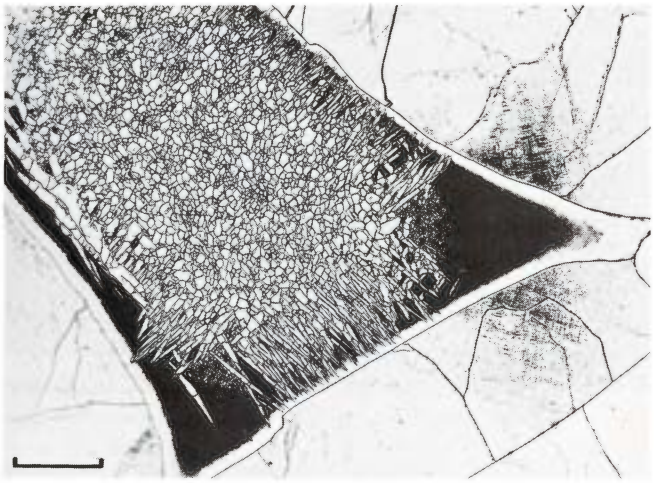

Figure 195. Cape York (Agpalilik) (Copenhagen no. 1967, 410). Net plessite with corners of black taenite. In the adjacent kamacite, slipplanes are decorated with minute particles, possibly phosphides, and appear dark. Etched. Scale bar 300 μ.

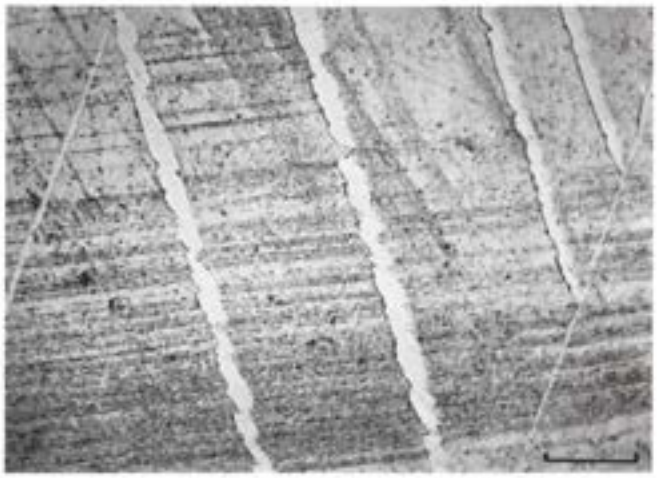

Figure 196. Kouga Mountains (Brit. Mus. 1916, 60). High magnification of an area with decorated sliplines, like that in Figure 195. The precipitates are submicroscopic; i.e., less than 0.3 μ in diameter. Etched. Scale bar 20 μ.

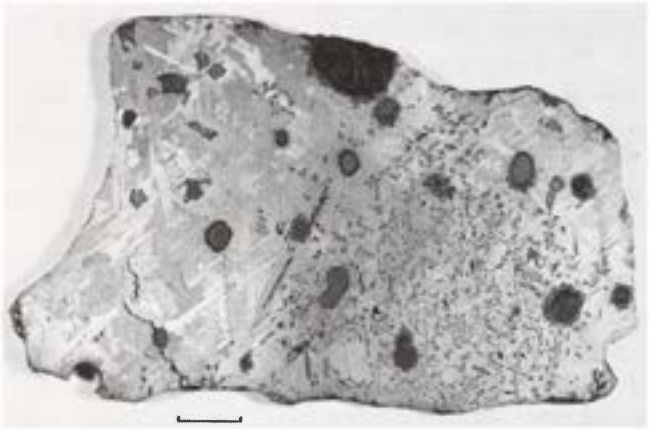

Figure 197. Canyon Diablo (U.S.N.M. no. 1705, the Rifle sample). Full slice showing graphite and graphite-troilite nodules. Rims of schreibersite and cohenite have precipitated upon them. The numerous skeleton crystals of schreibersite are enveloped in cohenite rims. Compare Figure 198. Etched. Scale bar 30 mm, S.I. neg. 44220.

b. In octahedrites with less than about 7.5% Ni, some grain boundary adjustment took place, i.e., favorably oriented kamacite grains advanced at the expense of adjacent less favorably oriented grains. Swathing kamacite rims grew into adjacent kamacite lamellae, kamacite lamellae grew into the kamacite of plessitic regions, etc. Since the taenite simultaneously became almost resorbed and secondary shock and annealing events often produced matte kamacite, the characteristic bulk Widmanstätten structure with straight lines and oriented sheen has sometimes become severely modified; see, e.g., Davis Mountains, Chilkoot, Campo del Cielo (group I), Bischtübe (group I) and Clark County (anomalous).

c. Troilite with chromium in solid solution precipitated daubreelite. The daubreelite lamellae exsolved parallel to the (0001) planes of the hexagonal troilite. It appears that the finest exsolution lamellae formed at low temperature within small, chromium-rich sulfide particles.

d. Carlsbergite particles – i.e., chromium nitrides – precipitated in the kamacite lamellae and along α - γ and other heterogeneous interfaces. They were cogenetic with or slightly earlier than the rhabdites, which often envelop them.

VI. Very minor changes occurred in the microstructure below about 500° C. The kamacite became veined; i.e., was subdivided into numerous subgrains which are slightly tilted with respect to each other. The shift of orientation across a subboundary is usually less than 1°, as may – among other things – be seen by the very slight shift in the direction of the subsequently introduced Neumann bands. Subboundaries arise through the running together of dislocations and were probably caused by relatively mild conditions of hot-working. The subboundaries are present in virtually all iron meteorites, irrespective of chemical group. Minute phosphide, and sometimes carbide and

nitride, particles (~ 1 μ) have usually precipitated upon the dislocations of the subboundaries.

The taenite rims with 30-40% Ni in solid solution had now also started to decompose to stained (or cloudy) taenite; i.e., submicroscopic duplex $\alpha + \gamma$ mixtures. Carbon probably migrated somewhat; it appears that taenite within the same polished section may contain rather different carbon concentrations.

One of the last reactions to occur was the decomposition of part of the retained taenite to α_2, or directly or indirectly, to $\alpha + \gamma$. Massalski et al. (1966) have treated this aspect thoroughly. The problem is extremely involved, and it may be that much of the taenite remained as undecomposed, metastable austenite until very late when shock pressures associated with the breakup of the parent body altered it.

The transformation of retained taenite to α_2 was associated with a small volume increase. Thereby plastic deformations were induced into the adjacent kamacite to a distance of 0.1-0.5 mm from the transformed region. As the system further cooled the sliplines in the kamacite were partially preserved by precipitation of fine particles (< 1 μ) of phosphide or austenite; see, e.g., Thule.

The solid state transformations in troilite at low temperatures and the exsolution of daubreelite lamellae from troilite possibly caused additional deformation of the adjacent kamacite. As above, fine particles might later precipitate in the strained ferrite phase.

Modifications Caused by Other Compositions

Although developed above for group IIIA-IIIB meteorites, stages I-VI may be discerned in most iron meteorites. In group I, which is anomalously rich in carbon and silicates, the first stage (completely molten metal) is not well developed, and is perhaps absent. However, the sulfides have been melted and a significant part of the carbon has accumulated here as graphite. A part of the carbon remained in solid solution in the taenite until, during stage III-IV, it precipitated as cliftonitic graphite. During stage IV-V carbon precipitated as cohenite which formed massive rims, nucleated by schreibersite, or formed elongated, branched millimeter-sized cohenite crystals in the α-lamellae. Finally, a small portion precipitated during stage VI as haxonite, mainly within pearlitic and spheroidized plessite.

In group II, the hexahedrites, stage Va is not well developed. Either it was already entirely wiped out when, at about 600° C, the nickel-poor material (< 5.8% Ni) passed into homogeneous α-phase, or the Widmanstätten structure was never present. Certain observations indicate

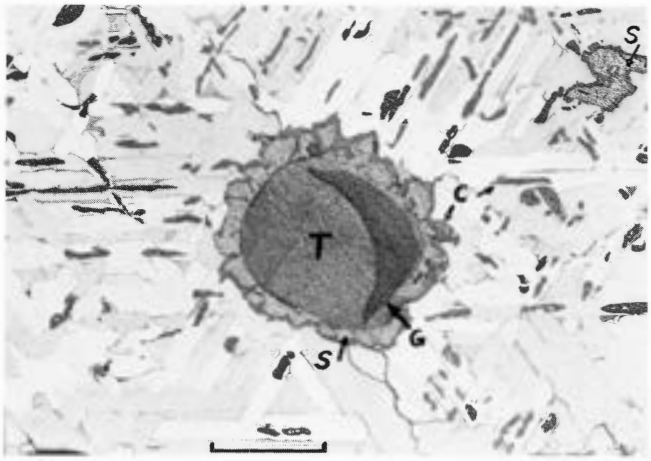

Figure 198. Detail of Figure 197, turned through 90°. Troilite T, graphite G, schreibersite S, and cohenite C in a coarse octahedrite of group I. Etched. Scale bar 10 mm. S.I. neg. 44220-C.

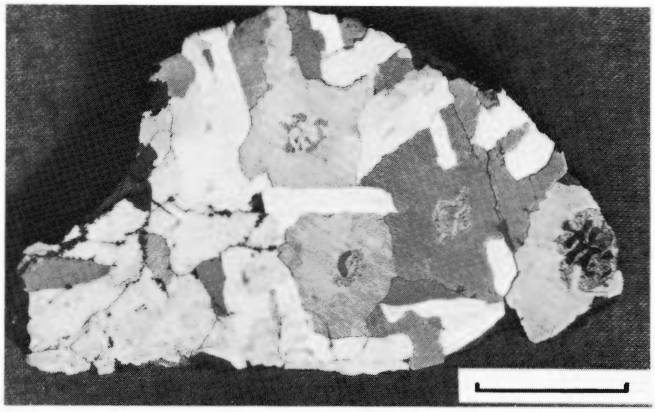

Figure 199. Santa Luzia (U.S.N.M. no. 1219). A coarsest octahedrite of group IIB. Swathing kamacite grew around four large troilite-schreibersite inclusions before the remaining taenite transformed to a Widmanstätten pattern. Etched. Scale bar 30 mm. S.I. neg. 32948.

that the hexahedrites may have formed from high temperature $\alpha + \gamma$ mixtures by (massive) growth of kamacite from early, homogeneous or heterogeneous nuclei. In meteorites with slightly higher average nickel contents, e.g., group IIB with about 6% Ni, it appears that both transformation mechanisms were active. In for example Sikhote-Alin, Santa Luzia, Tombigbee and New Baltimore α nucleated and grew around primary schreibersite and troilite bodies, and, in competition, homogeneous Widmanstätten transformation occurred a few centimeters away with the result that the structure is now a mixture of hexahedrite and coarsely crystalline octahedrite structures.